Article

A Feasibility Study of a Novel Piezo MEMS Tweezer for Soft Materials Characterization

Fabio Botta *[ID], **Andrea Rossi** [ID] **and Nicola Pio Belfiore** [ID]

Dipartimento di Ingegneria, Università degli Studi Roma Tre, Via della Vasca Navale, 79, 00146 Roma, Italy; andrea.rossi@uniroma3.it (A.R.); nicolapio.belfiore@uniroma3.it (N.P.B.)
* Correspondence: fabio.botta@uniroma3.it; Tel.: +39-06-57333491

check for updates

Abstract: The opportunity to know the status of a soft tissue (ST) in situ can be very useful for microsurgery or early diagnosis. Since normal and diseased tissues have different mechanical characteristics, many systems have been developed to carry out such measurements locally. Among them, MEMS tweezers are very relevant for their efficiency and relative simplicity compared to the other systems. In this paper a novel piezoelectric MEMS tweezer for soft materials analysis and characterization is presented. A theoretical approach has developed in order to carry out the values of the stiffness, the equivalent Young's modulus, and the viscous damping coefficients of the analyzed samples. The method has been validated by using both Finite Element Analysis and data from the literature.

---

1. Introduction

Early diagnosis is crucial to prevent disease progressions [1]. The correlation between the mechanical characteristics of a soft tissue and its status has been highlighted by several studies in many cell types like cancer cells, epithelial cells and laminopathies associated with diseases of the nuclear membrane [2]. In cancer cells, for example, the malignant transformation influences the mechanical properties by disruption and/or reorganization of cytoskeleton [3]. The stiffness, the elastic modulus, and the dynamic viscosity are among the most commonly used mechanical quantities to evaluate the state of a soft tissue. However the possibility to identify a diseased soft tissue in situ, at the microscale, can increase significantly the possibility of the cure.

Different techniques are used to perform such measurements as micropipette aspiration [4], magnetic bead twisting [5], atomic force microscopy [6], optical tweezers [7] or mechanical tweezers [8]. In recent years, researchers focused on the developing of micro-electro-mechanical systems (MEMS) tweezers because of their efficiency and relative simplicity with respect to other systems [9]. New gripping tweezers have been built taking cue from the kinematics of articulated mechanisms [10] as the property of parallelograms [11–15]. More complex motion, with an increasing of the number of degrees of freedom, can be obtained adopting the concept of lumped compliance. In fact, concentrated flexibility has been used in flexure hinges in several investigations [16–20]. In order to improve the displacement accuracy and to lower the stress levels in the flexible elements a new conjugate surfaces flexure hinge (CSFH) flexure has been proposed [21–25] and optimized [26,27]. The system has shown promising results in terms of of versatility and applicability to different types of tissue [28]. Thanks to their high level of miniaturization, MEMS-Technology based tweezers can be employed also in minimal invasive [29–31] or gastrointestinal surgery [32], and more generally speaking, in endoluminal surgery, for example, in TEM [33–35].

The actuation of the tweezer can be obtained by different systems, such as linear electrostatic actuators [36,37], rotary electrostatic actuators [38,39] or electrothermal actuation [40–46]. However the advent of smart materials in the last decades has greatly increased the possibilities of development of new smart structures [47–49] with the ability, not possible for the traditional systems, to adapt to external conditions variations. Because of their speed of response, low power consumption and high operating bandwidth the piezoelectric materials are, among the smart materials, the most promising ones for active vibration control [50–53] and MEMS applications [54]. However the research in the latter field mainly focuses on the energy harvesting [55–58] or MEMS tweezers for manipulating micro-objects and microassembly [59–61].

This paper presents the design of a novel piezoMEMS tweezer for the analysis and characterization of soft materials. Each jaw can be built as a sandwich composite beam and activated by an electric field.

The tweezer is supposed to be force controlled because the piezoelectric materials produce a stress proportional to the applied electrical field. Furthermore, a sensor is supposed to be integrated into the structure for displacement control. This gives rise to improve the analysis of the cell properties. In fact, the displacement-controlled actuator is able to identify the beginning of a rupture during straining or softening, while a force-controlled system maintains a constant force regardless of the required displacement [62]. The action of the piezoelectric material has been modeled by the Pin Force Model [63].

By applying symmetric electric fields to the composite jaws, they will bend in opposite directions allowing the gripping of the soft tissue.

A new mathematical model to measure the stiffness, the equivalent Young's modulus, and the viscous damping coefficient of the soft tissue has been developed. The model has been tested on three different soft test specimens and the results were in good agreement with those obtained by COMSOL finite elements code.

2. The Adopted Piezo-Mems Microgripper

The purpose of this paper is to develop a theoretical model of a piezo-MEMS microgripper, which can be used to characterize a grasped sample tissue. Therefore, the actual fabrication process of this instrument will not be herein considered. However, for the sake of completeness, a selection of possible materials and technological processes is briefly recalled.

In the last decades, several actuation methods have been proposed to induce motion in MEMS devices such as electrostatic, thermal and piezoelectric. The electrostatic devices are widely adopted but the piezoelectric MEMS's offer some attractive advantages: lower power consumption, broader bandwidth and approximately ten times lower voltages to obtain the same given displacement [64]. Furthermore the piezoelectric materials can be manufactured using the same MEMS conventional technologies and for this reason these materials have been preferred to develop piezo-MEMS devices in the last decades. Typical applications include vibration energy harvesters [65,66], resonators [67], capacitors [68], micro sensors/actuators [69,70], micromachined ultrasonic transducer [71], gyroscopic sensors [72], microlens [73,74], 1D and 2D micro-scanners [75,76].

The piezoelectric materials can be gathered into two groups: ferroelectric (lead zirconate titanate, PZT compounds) and non-ferroelectric (ZnO and AlN). The piezoelectric characteristics (piezoelectric coefficient, Q factor, dielectric constant, etc.) rely on the crystalline structure. In fact ZnO and AlN thin-films show wurtzite structure that entails lower piezoelectricity if compared to PZT materials (perovskite structure). Nevertheless ZnO and AlN exhibit large mechanical stiffness, high Q factor and do not require a polarization process so they can be attractive for sensors applications. PZT thin-films provide high piezoelectric properties, lower cost and stability against temperature but require a poling process before using the piezo-MEMS device [77]. The electric field poling direction depends on the functional configuration of the piezo-MEMS.

Usually the piezoelectric MEMS actuators/sensors are based on cantilever structures and the number of active layers identifies their working configuration:

- unimorph (one piezoelectric layer coupled with an inactive structural layer) or
- bimorph (a structural layer sandwiched by two active layers).

When a PZT bimorph bending beam and the transverse piezoelectric effect (d_{31}) are considered, the PZT layers must be poled in opposite directions in order to maximize the bending action. Then the electrodes of the PZT layers in contact with the structural layer share the same electric potential, whereas the outer electrodes share the same opposite sign potential (see Section 3). The design and fabrication process of piezo-MEMS devices have been extensively explored for the above mentioned unimorph and bimorph cantilever configurations using the aforementioned materials:
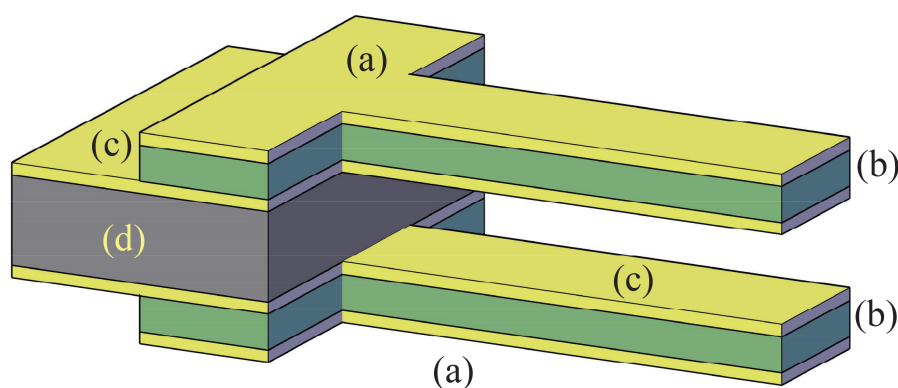
- AlN [67,68,71];
- ZnO [70]; and
- PZT [66,69,75,78].

Various technologies can be applied to deposit piezoelectric thin-films such as

- pulsed laser deposition (PLD);
- chemical vapour deposition (CVD);
- screen printing;
- sol-gel and
- radio frequency sputtering.

Usually the sol-gel and sputtering methods are the preferred ones both for research and commercial production because they allow the piezoelectric thin-film to be homogeneously deposited on large Si wafers [79]. The beam structural layer can be metal-based or silicon-based and the etching processes could be accomplished relying on conventional techniques (RIE, D-RIE, ECR).
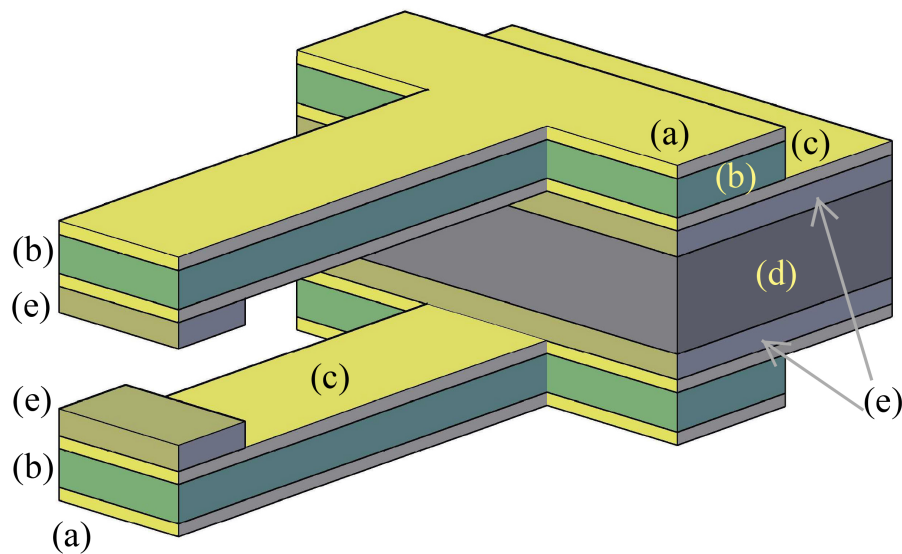
A schematic view of the target piezo-MEMS tweezer is qualitatively depicted in Figure 1. The system can be obtained by using a multilayer wafer that can be built by using the above mentioned techniques. At the end of the process, the whole microsystem is composed of two bimorph beams (**a**)-(**b**)-(**c**) (see Figure 1). The two bimorph beams are supported by the handle layer (**d**). The specific steps of the process (deposition, etching, exposure, etc.) will depend on the peculiar materials and technology selected for the construction. In the case under study, the system is conceived in such a way that the mask geometry could be quite elementary for any etching step.

Figure 1. A schematic view of the microsystem: outer layers with a same voltage V_0 (**a**); structural material for the beams (**b**); internal layers with voltage V_i (**c**) and structural layer for the handle (**d**).

Another possible layout is represented in Figure 2, where two new layers (**e**) have been added with respect to the previous example of fabrication. Layers (**a**), (**b**), (**c**), and (**d**) have the same function as described for the previous layout. The second design is better for the operational aspects because a clamping tooth has been added for each jaw. However, these two teeth are more difficult to obtain

during the process because they require at least two more deposition layers (**e**) and also a more complex series of intermediate etching-deposition steps that depend on the selected materials.

Figure 2. An alternative layout for the microgripper: outer layers with a same voltage V_0 (**a**); structural material for the beams (**b**); internal layers with voltage V_i (**c**) and structural layer for the handle (**d**).

3. Modeling Piezoelectric Actions on the Microbeams

Concerning the piezoelectric actions, many studies [63,80–82] have confirmed that, under certain assumptions (piezoelectric plates are perfectly bonded to the structure, the ratio between their thickness and the thickness of the beam is very low and their inertia and mass negligible with respect to those of the beam) the stresses applied to the beam can be considered as they were concentrated at the piezoelectric plate ends. Moreover, if the electric field to the upper plate is opposite in sign to the one applied to the lower plate, such action is equivalent to a flexural moment (see Figure 3) applied to the end of the beam of magnitude equal to:

$$M_a(t) = \frac{\psi}{6+\psi} E_a c T_a T_b \Lambda(t) \tag{1}$$

with

$$\begin{cases} \Lambda(t) = \frac{d_{31}}{T_a} V(t) \\[2mm] \psi = \frac{E_b T_b}{E_a T_a} \end{cases} \tag{2}$$

Figure 3. Piezoelectric action (PIN force model).

By activating the piezoelectric plates pairs on the two jaws-beams of the tweezer in opposite manner the two moments M_a will have opposite sign and the beams will bend in opposite direction allowing the gripper to grasp the soft tissue, as depicted in Figure 4.
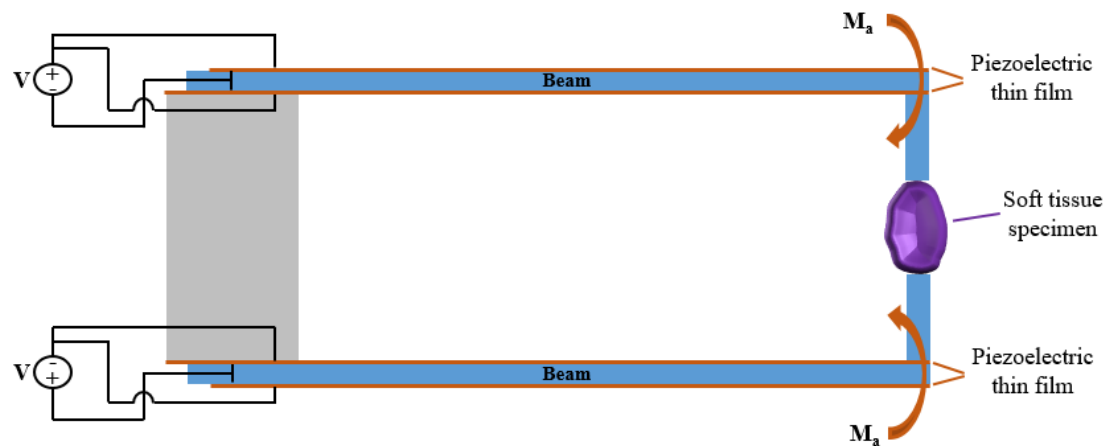
Figure 4. PiezoMEMS grip of the soft tissue.

3.1. Static Model

The value of the stiffness K_{ST} and of the equivalent Young's modulus E_{ST} can be established by a static test with a constant voltage V_0 applied to the piezoelectric plates: $V(t) = V_0$. In this case, the bending of the beams will cause the compression of the soft tissue and consequently a reaction force F_{ST} will be applied from the soft tissue to the beams, through the clamp teeth (see Figure 5).
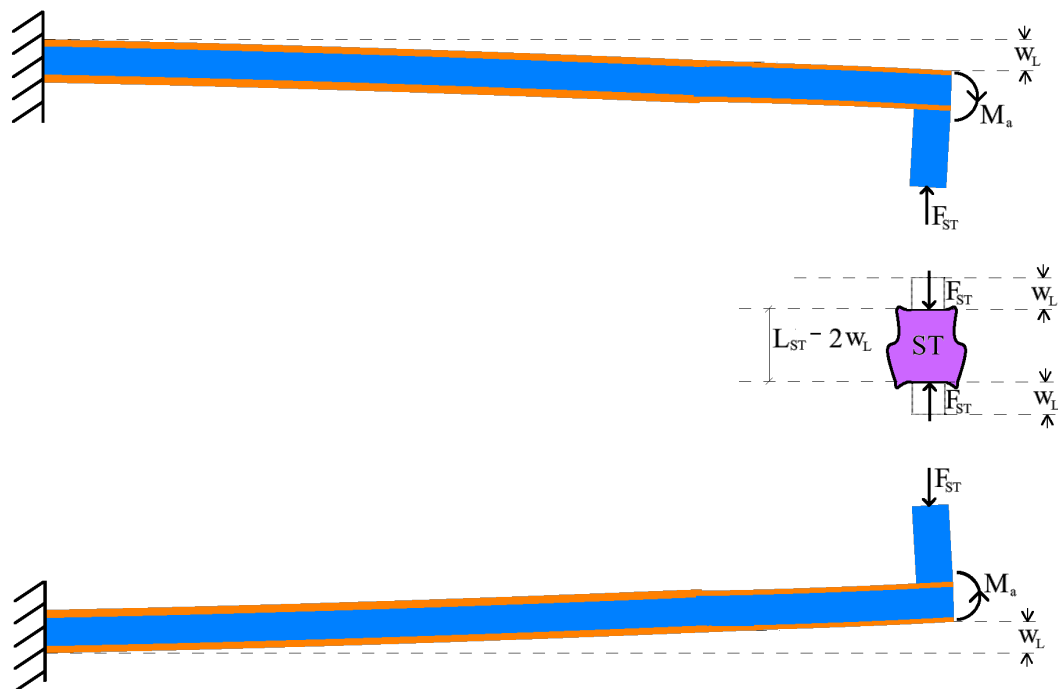

Figure 5. Scheme for the calculation of the tip displacement.

Considering that the Euler Bernoulli model is appropriate for the present case because of the high length-to-thickness aspect ratio of the beams, the tip deflection:

$$w_L = \frac{M_a L^2}{2 E_b I_b} - \frac{F_{ST} L^3}{3 E_b I_b} \, , \tag{3}$$

is due to a combination of the loads F_{ST} and M_a. Therefore, the first load

$$F_{ST} = \frac{3E_b I_b}{L^3} \left(\frac{M_a L^2}{2E_b I_b} - w_L \right) \tag{4}$$

can be obtained by measuring w_L.

Due to the high value of the axial stiffness of the clamp teeth, the deflection w_L can be considered equal to the axial displacement of the soft tissue (see Figure 5) so that the axial strain

$$\epsilon_{ST} = \frac{2w_L}{L_{ST}} \tag{5}$$

is calculated.

Under the assumption of linear elastic behavior for the soft tissue (ST), the relationship between the normal stress σ_{ST} applied to the cross section of the soft tissue and ϵ_{ST} can be written as:

$$\sigma_{ST} = \frac{F_{ST}}{S_{ST}} = E_{ST} \frac{2w_L}{L_{ST}} \tag{6}$$

from which the equivalent Young's modulus

$$E_{ST} = \frac{F_{ST} L_{ST}}{2S_{ST} w_L} \tag{7}$$

is evaluated. Moreover, the stiffness

$$K_{ST} = \frac{2E_{ST} S_{ST}}{L_{ST}} \tag{8}$$

is calculated given the dimensions of the ST sample.

3.2. Dynamics Model

To determine the value of the viscous damping C_{ST}, a dynamic test has been conceived by applying a variable harmonic excitation voltage $V(t) = V_0 sin(\omega t)$.

By referring to δL_{int}, δL_{in}, δL_a and δL_{ST} as the virtual works of internal, inertial, actuator and ST forces, respectively, and to δL_{in_m} as the virtual work of the inertial forces of the clamp teeth, the virtual work principle can be written as:
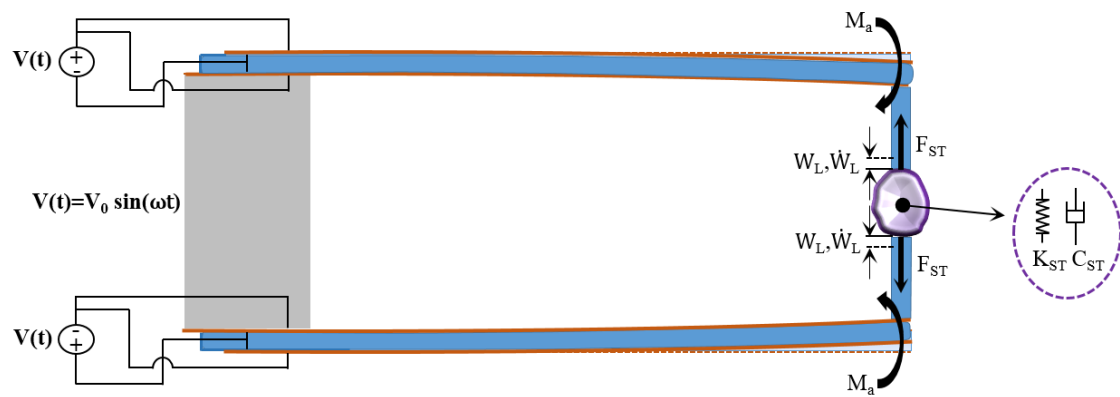
$$\delta L_{int} = \delta L_{in} + \delta L_a + \delta L_{in_m} + \delta L_{ST} \tag{9}$$

where (the quantities over signed by a tilde are virtual quantities):

$$\begin{cases} \delta L_{int} = E_b I_b \int_0^L \frac{\partial^2 w}{\partial x^2} \frac{\partial^2 \widetilde{w}}{\partial x^2} dx \\[2mm] \delta L_{in} = -\rho S \int_0^L \frac{\partial^2 w}{\partial t^2} \, \widetilde{w} \, dx \\[2mm] \delta L_a = M_a \frac{\partial \widetilde{w}}{\partial x} \Big|_{x=L} \\[2mm] \delta L_{in_m} = -m \frac{\partial^2 w_L}{\partial t^2} \, \widetilde{w_L} \\[2mm] \delta L_{ST} = F_{ST} \, \widetilde{w_L} \end{cases} \tag{10}$$

with (see Figure 6):

$$F_{ST} = K_{ST} w_L + C_{ST} \, \dot{w}_L \tag{11}$$

Figure 6. Scheme for the calculation of the stiffness and viscous damping of the soft tissue.

The viscous damping coefficient C_{ST} can be identified by measuring the amplitude $|w_L|$ in correspondence of the *i*-th vibration mode of the structure that has been excited by means of the piezoelectric elements, where the flexural modes of the beams are obtained as

$$\varphi(x) = B_1 \sin(\lambda x) + B_2 \cos(\lambda x) + B_3 \sinh(\lambda x) + B_4 \cosh(\lambda x) \tag{12}$$

with

$$
\begin{cases}
\varphi(0) = 0 \\[2mm]
\left. \dfrac{\partial \varphi(x)}{\partial x} \right|_{x=0} = 0 \\[2mm]
\left. \dfrac{\partial^2 \varphi(x)}{\partial x^2} \right|_{x=L} = 0 \\[2mm]
EI \left. \dfrac{\partial^3 \varphi(x)}{\partial x^3} \right|_{x=L} = K_{ST} \varphi(L) - \omega^2 m \varphi(L)
\end{cases}
\tag{13}
$$

By substituting Equation (12) in (13), a system of four equations in four unknowns (B_1, B_2, B_3, B_4) is obtained. The eigenfrequencies are obtained setting to zero the determinant of the matrix coefficient (with $\omega^2 = \lambda^4 \frac{EI}{\rho S}$) and then the eigenmodes can be calculated.

The *i*-th flexural mode can be excited by applying a potential function

$$V(t) = V_0 \sin(\omega_i t) \tag{14}$$

where $\varphi_i(x)$ and ω_i are the *i*-th flexural mode and its related frequency, respectively. In these conditions the displacement $w(x, t)$ and the virtual displacement $\tilde{w}(x, t)$ can be written as:

$$
\begin{cases}
w(x, t) = A_i(t) \varphi_i(x) \\[2mm]
\tilde{w}(x, t) = \varphi_i(x)
\end{cases}
\tag{15}
$$

By substituting Equations (15) and (10) in (9), the following equation is obtained:

$$
\begin{aligned}
E_b I_b A_i(t) \int_0^L \frac{\partial^2 \varphi_i(x)}{\partial x^2}^2 dx &= -\rho S \, \ddot{A}_i(t) \int_0^L \varphi_i(x)^2 dx - m \, \ddot{A}_i(t) \, \varphi_i(L)^2 + \\
&\quad + M_a \left. \frac{\partial \varphi_i(x)}{\partial x} \right|_{x=L} - K_{ST} A_i(t) \varphi_i(L)^2 - C_{ST} \, \dot{A}_i(t) \, \varphi_i(L)^2
\end{aligned}
\tag{16}
$$

assuming (see Equation (1)):

$$
\begin{cases}
M = \rho S \int_0^L \varphi_i(x)^2 dx + m \varphi_i(L)^2 \\[2mm]
C = C_{ST} \varphi_i(L)^2 \\[2mm]
K = E_b I_b \int_0^L \dfrac{\partial^2 \varphi_i(x)}{\partial x^2}^2 dx + K_{ST} \varphi_i(L)^2 \\[2mm]
Q = \dfrac{\psi}{6+\psi} E_a c T_b d_{31} \left. \dfrac{\partial \varphi_i(x)}{\partial x}\right|_{x=L} V_0
\end{cases}
\tag{17}
$$

and therefore Equation (16) becomes:

$$
M \ddot{A}_i(t) + C \dot{A}_i(t) + K A_i(t) = Q \sin(\omega_i t)
\tag{18}
$$

By neglecting the transient part (see Equation (15.1)), the amplitude of the free end displacement is:

$$
\left| w_L \right| = A_{i_f} \varphi_i(L)
\tag{19}
$$

where

$$
A_{i_f} = \frac{Q}{C \omega_i}.
\tag{20}
$$

Finally, the damping coefficient of the soft tissue

$$
C_{ST} = \frac{Q}{\left| w_L \right| \omega_i \varphi_i(L)}
\tag{21}
$$

can be found from Equation (17.2).

4. Results and Discussion

To validate the proposed model, numerical simulations have been done. The dimensions and the material characteristics are summarized in Table 1:
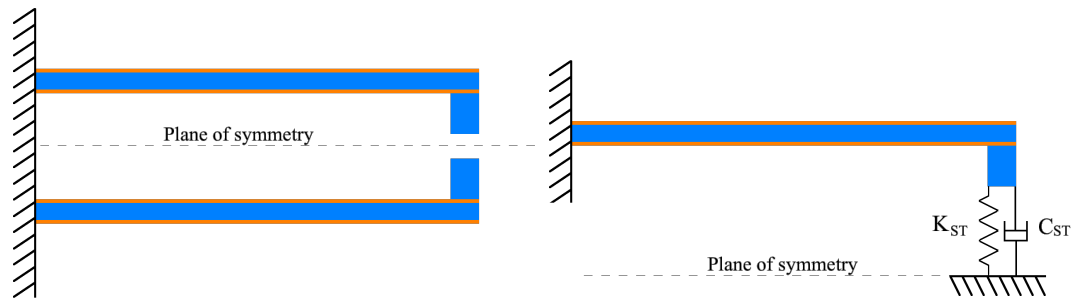
Table 1. Beams, piezoelectric plates and end masses specifications; lengths are expressed in µm.

	Material	Length	Thickness	Width	Young's mod. [GPa]	Density $[\mathrm{kg/m^3}]$
Beams	Silicon	750	2	80	170	2329
Piezoel. pl.	AlN	750	$2 * 10^{-2}$	80	350	3300
Clamp teeth	Silicon	36	7.5	80	170	2329

In this work, the FEM results have been chosen as the reference values. Three typical soft tissues (liver, muscle and uterus) of known characteristics [83], have been considered. The value of the beam tip displacement, obtained by the FEM simulations, has been included in the mathematical model to calculate the equivalent Young's modulus and the viscous damping coefficient. The ST sample stiffness can be calculated by means of Equation (8). The values of the Young's modulus and the viscous coefficients reported in the literature have been compared with the ones calculated by the new method. Because of the symmetry of the structure with respect to its mid-plane (see Figure 7) only the upper part has been considered in the simulations.

In Table 2 the results of the static simulations, obtained by the above described procedure, have been reported. It is possible to observe that the model results are in good agreement with the real values with a percentage error less than 6% in all the cases.

Figure 7. Scheme used for the simulations.

Table 2. Comparison between the actual Young's modules and those obtained by the model; E_{mm} is the Young's modulus obtained by the mathematical model.

	E [kPa]	E_{mm} [kPa]	*Err* %
Liver	10	9.47	5.3%
Muscle	20	19.43	2.8%
Uterus	30	29.64	1.2 %

To obtain the viscous damping coefficient, dynamics simulations are necessary. As described above, the chosen strategy consists in exciting, by the piezoelectric plates, the *i*-th mode of the structure, in order to obtain the amplitude of the free end displacement $|w_L|$ and then in including this in the model.

A comparison between the eigenfrequencies obtained by the COMSOL FEM code and the proposed model is reported in Table 3.

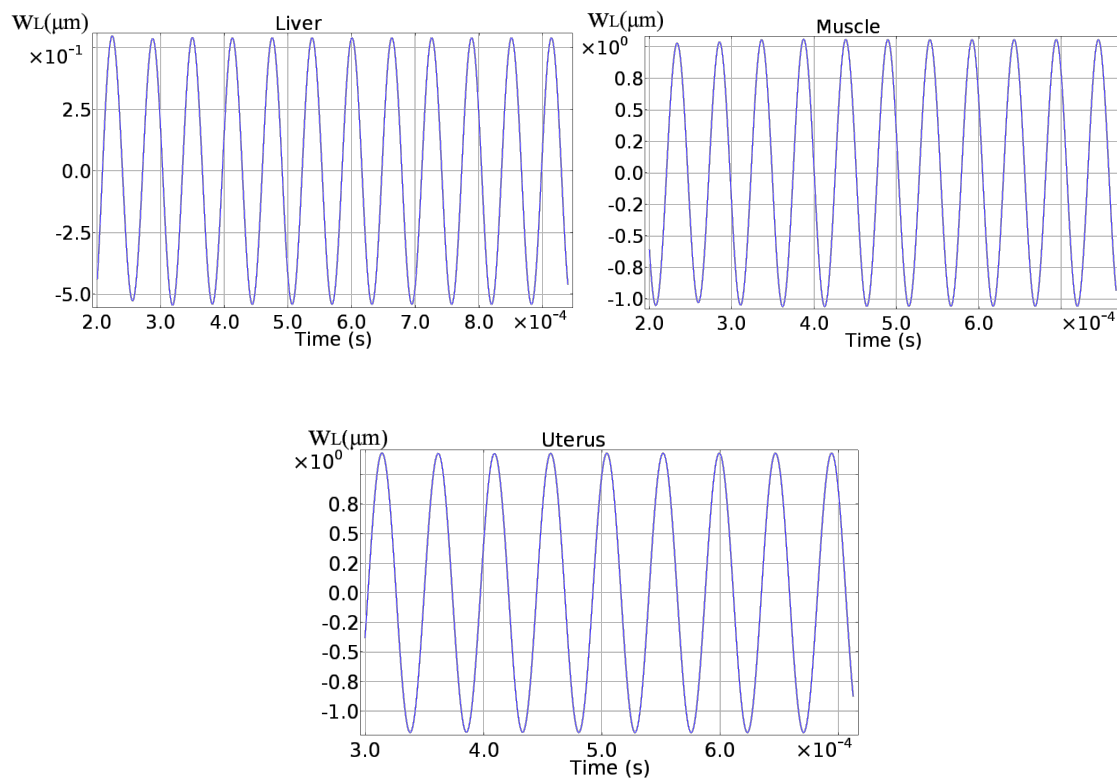**Table 3.** Comparison between the eigenfrequencies obtained by the COMSOL FEM code and the proposed model.

	Liver		
	FEM	*Model*	*Err%*
$f_1[Hz]$	15,523.50	15,856.40	2.14%
$f_2[Hz]$	30,701.40	29,487.60	3.95%
$f_3[Hz]$	82,116.70	75,668.50	7.85%
$f_4[Hz]$	162,877.10	151,620.00	6.91%
	Muscle		
	FEM	*Model*	*Err%*
$f_1[Hz]$	18,768.20	18,686.20	0.44%
$f_2[Hz]$	35,437.60	34,681.70	2.13%
$f_3[Hz]$	82,674.80	76,297.90	7.71%
$f_4[Hz]$	162,995.20	151,781	6.88%
	Uterus		
	FEM	*Model*	*Err%*
$f_1[Hz]$	20,066.80	19,721.70	1.72%
$f_2[Hz]$	40,190.2	39,660.70	1.32%
$f_3[Hz]$	83,255.70	77,038.00	7.47%
$f_4[Hz]$	163,118.00	151,949.00	6.85%

In the FEM simulations the first mode has been chosen to excite the structure with the values of the electrical potential reported in Table 4.

Table 4. Electrical potential used for the simulations.

	$V_0[V]$
Liver	8
Muscle	5
Uterus	5

By neglecting the initial transient part, the axial displacements for the various soft tissues have been reported in Figure 8.

Figure 8. Axial displacement for the various soft tissues.

Finally, the comparison between the actual viscous damping coefficients and those obtained by the model results have been highlighted in Table 5.

Table 5. Comparison between the effective viscous damping and those obtained by the model.

	$C[Ns/m]$	$C_{mm}[Ns/m]$	$Err\%$
Liver	$3.07 * 10^{-5}$	$2.94 * 10^{-5}$	4.2%
Muscle	$5.09 * 10^{-5}$	$4.98 * 10^{-5}$	2.2%
Uterus	$7.14 * 10^{-5}$	$7.26 * 10^{-5}$	1.7%

A good agreement between the relative coefficients is also observed with a percentage error always less than 5%.

5. Conclusions

In this paper a novel piezo MEMS tweezer for soft materials characterization has been proposed. The tweezer mechanical structure is compatible with the known fabrication processes. A new mathematical model to calculate the stiffness, the equivalent Young's modulus and the viscous damping coefficient of the soft tissues is suggested. The method has been tested by comparing its results with Finite Element

Analysis based on experimental data from the literature. The two sets of data are in good agreement with a difference less than 6% in all the considered cases.

Author Contributions: F.B. has designed and developed the mathematical model. A.R. and F.B. carried out the numerical simulations. N.P.B. has reviewed the theoretical approach and the compatibility of the structure with some technological fabrication process.

Conflicts of Interest: The authors declare no conflict of interest.

Abbreviations

The following abbreviations are used in this manuscript:

C	damping coefficient
C_{ST}	damping coefficient of the soft tissue
d_{31}	piezoelectric coefficient
E_a	Young's modulus of the piezoelectric material
E_b	Young's modulus of the beam
E_{ST}	equivalent Young's modulus of the soft tissue
F_{ST}	force applied from the soft tissue to the tweezers
I_b	inertia moment of the beam
K	stiffness coefficient
K_{ST}	stiffness coefficient of the soft tissue
L	beam length
m	mass applied at the end of the tweezer
M_a	piezoelectric bending moment
M	mass coefficient
S_{ST}	cross-sectional area of the soft tissue
ST	soft tissue
T_a	piezoelectric thickness
T_b	beam thickness
V	electric potential applied to the piezoelectric plates
w	transverse displacement
w_L	transverse displacement of the free end
$\tilde{w}$	virtual transverse displacement
$\phi_i(x)$	i-th flexural mode of the beam
ρ	mass density of the beam
ω_i	natural frequency of the i-th flexural mode

References

1. Tang, M.; Xia, L.; Wei, D.; Yan, S.; Du, C.; Cui, H.L. Distinguishing Different Cancerous Human Cells by Raman Spectroscopy Based on Discriminant Analysis Methods. *Appl. Sci.* **2017**, *7*, 900. [CrossRef]
2. Rianna, C.; Radmacher, M. Comparison of viscoelastic properties of cancer and normal thyroid cells on different stiffness substrates. *Eur. Biophys. J.* **2017**, *46*, 309–324. [CrossRef] [PubMed]
3. Lekka, M.; Gil, D.; Pogoda, K.; Dulińska-Litewka, J.; Jach, R.; Gostek, J.; Klymenko, O.; Prauzner-Bechcicki, S.; Stachura, Z.; Wiltowska-Zuber, J.; et al. Cancer cell detection in tissue sections using AFM. *Arch. Biochem. Biophys.* **2012**, *518*, 151–156. [CrossRef] [PubMed]
4. Discher, D.E.; Boal, D.H.; Boey, S.K. Simulations of the erythrocyte cytoskeleton at large deformation. II. Micropipette aspiration. *Biophys. J.* **1998**, *75*, 1584–1597. [CrossRef]
5. Bausch, A.R.; Ziemann, F.; Boulbitch, A.A.; Jacobson, K.; Sackmann, E. Local measurements of viscoelastic parameters of adherent cell surfaces by magnetic bead microrheometry. *Biophys. J.* **1998**, *75*, 2038–2049. [CrossRef]
6. Weisenhorn, A.L.; Khorsandi, M.; Kasas, S.; Gotzos, V.; Butt, H.J. Deformation and height anomaly of soft surfaces studied with an AFM. *Nanotechnology* **1993**, *4*, 106. [CrossRef]
7. Guck, J.; Ananthakrishnan, R.; Cunningham, C.C.; Käs, J. Stretching biological cells with light. *J. Phys. Condens. Matter* **2002**, *14*, 4843. [CrossRef]

8. Adldoost, H.; Jouibary, B.R.; Zabihollah, A. Design of SMA micro-gripper for minimally invasive surgery. In Proceedings of the 2012 19th Iranian Conference of Biomedical Engineering, Tehran, Iran, 20–21 December 2012.

9. Botta, F.; Verotti, M.; Bagolini, A.; Bellutti, P.; Belfiore, N.P. Mechanical response of four-bar linkage microgrippers with bidirectional electrostatic actuation. *Actuators* **2018**, *7*, 78. [CrossRef]

10. Tsai, Y.C.; Lei, S.H.; Sudin, H. Design and analysis of planar compliant microgripper based on kinematic approach. *J. Micromech. Microeng.* **2004**, *15*, 143. . [CrossRef]

11. Wierzbicki, R.; Adda, C.; Hotzendorfer, H. Electrostatic silicon microgripper with low voltage of actuation. In Proceedings of the 2007 International Symposium on Micro-NanoMechatronics and Human Science, Nagoya, Japan, 11–14 November 2007.

12. Hamedi, M.; Salimi, P.; Vismeh, M. Simulation and experimental investigation of a novel electrostatic microgripper system. *Microelectron. Eng.* **2012**, *98*, 467–471. [CrossRef]

13. Piriyanont, B.; Moheimani, S.R.; Bazaei, A. Design and control of a MEMS micro-gripper with integrated electro-thermal force sensor. In Proceedings of the 2013 Australian Control Conference, Fremantle, WA, Australia, 4–5 November 2013.

14. Wierzbicki, R.; Houston, K.; Heerlein, H.; Barth, W.; Debski, T.; Eisinberg, A.; Dario, P. Design and fabrication of an electrostatically driven microgripper for blood vessel manipulation. *Microelectron. Eng.* **2006**, *83*, 1651–1654. [CrossRef]

15. Zhang, Y.; Chen, B.K.; Liu, X.; Sun, Y. Autonomous robotic pick-and-place of microobjects. *IEEE Trans. Robot.* **2010**, *26*, 200–207. [CrossRef]

16. Scalari, G.; Eisinberg, A.; Mazzoni, M.; Menciassi, A.; Dario, P. A sensorized μelectro discharge machined superelastic alloy microgripper for micromanipulation. In Proceedings of the IEEE/RSJ International Conference on Intelligent Robots and Systems, Lausanne, Switzerland, 30 September–4 October 2002; pp. 1591–1595.

17. Greminger, M.A.; Sezen, A.S.; Nelson, B.J. A four degree of freedom MEMS microgripper with novel bi-directional thermal actuators. In Proceedings of the 2005 IEEE/RSJ International Conference on Intelligent Robots and Systems, Edmonton, AB, Canada, 2–6 August 2005.

18. Chang, R.J.; Chen, C.C. Using microgripper for adhesive bonding in automatic microassembly system. In Proceedings of the International Conference on Mechatronics and Automation, Harbin, China, 5–8 August 2007.

19. Chronis, N.; Lee, L.P. Polymer MEMS-based microgripper for single cell manipulation. In Proceedings of the 17th IEEE International Conference on Micro Electro Mechanical Systems. Maastricht MEMS 2004 Technical Digest, Maastricht, The Netherlands, 25–29 January 2004.

20. Sun, X.; Chen, W.; Fatikow, S.; Tian, Y.; Zhou, R.; Zhang, J.; Mikczinski, M. A novel piezo-driven microgripper with a large jaw displacement. *Microsyst. Technol.* **2015**, *21*, 931–942. [CrossRef]

21. Belfiore, N.P.; Broggiato, G.B.; Verotti, M.; Balucani, M.; Crescenzi, R.; Bagolini, A.; Bellutti, P.; Boscardin, M. Simulation and construction of a mems CSFH based microgripper. *Int. J. Mech. Control* **2015**, *16*, 21–30.

22. Verotti, M.; Crescenzi, R.; Balucani, M.; Belfiore, N.P. MEMS-based conjugate surfaces flexure hinge. *J. Mech. Des.* **2015**, *137*, 012301. [CrossRef]

23. Cecchi, R.; Verotti, M.; Capata, R.; Dochshanov, A.; Broggiato, G.; Crescenzi, R.; Balucani, M.; Natali, S.; Razzano, G.; Lucchese, F.; et al. Development of micro-grippers for tissue and cell manipulation with direct morphological comparison. *Micromachines* **2015**, *6*, 1710–1728. [CrossRef]

24. Verotti, M.; Dochshanov, A.; Belfiore, N.P. Compliance Synthesis of CSFH MEMS-Based Microgrippers. *J. Mech. Des.* **2017**, *139*. [CrossRef]

25. Crescenzi, R.; Balucani, M.; Belfiore, N.P. Operational characterization of CSFH MEMS technology based hinges. *J. Micromech. Microeng.* **2018**, *28*, 055012. [CrossRef]

26. Verotti, M. Analysis of the center of rotation in primitive flexures: Uniform cantilever beams with constant curvature. *Mech. Mach. Theory* **2016**, *97*, 29–50. [CrossRef]

27. Verotti, M. Effect of initial curvature in uniform flexures on position accuracy. *Mech. Mach. Theory* **2018**, *119*, 106–118. [CrossRef]

28. Di Giamberardino, P.; Bagolini, A.; Bellutti, P.; Rudas, I.; Verotti, M.; Botta, F.; Belfiore, N.P. New MEMS tweezers for the viscoelastic characterization of soft materials at the microscale. *Micromachines* **2018**, *9*, 15. [CrossRef] [PubMed]

29. Ursi, P.; Santoro, A.; Gemini, A.; Arezzo, A.; Pironi, D.; Renzi, C.; Cirocchi, R.; Di Matteo, F.; Maturo, A.; D'Andrea, V.; et al. Comparison of outcomes following intersphincteric resection vs low anterior resection for low rectal cancer: A systematic review. *G. Di Chir.* **2018**, *39*, 123–142.

30. Balla, A.; Quaresima, S.; Ursi, P.; Seitaj, A.; Palmieri, L.; Badiali, D.; Paganini, A.M. Hiatoplasty with crura buttressing versus hiatoplasty alone during laparoscopic sleeve gastrectomy. *Gastroenterol. Res. Pract.* **2017**, *2017*. [CrossRef] [PubMed]

31. Cochetti, G.; Del Zingaro, M.; Boni, A.; Cocca, D.; Panciarola, M.; Tiezzi, A.; Gaudio, G.; Balzarini, F.; Ursi, P.; Mearini, E. Colovesical fistula: Review on conservative management, surgical techniques and minimally invasive approaches. *G. Di Chir.* **2018**, *39*, 195–207.

32. Popivanov, G.; Tabakov, M.; Mantese, G.; Cirocchi, R.; Piccinini, I.; D'Andrea, V.; Covarelli, P.; Boselli, C.; Barberini, F.; Tabola, R.; et al. Surgical treatment of gastrointestinal stromal tumors of the duodenum: A literature review. *Transl. Gastroenterol. Hepatol.* **2018**, *3*. [CrossRef] [PubMed]

33. Paci, M.; Scoglio, D.; Ursi, P.; Barchetti, L.; Fabiani, B.; Ascoli, G.; Lezoche, G. Transanal Endocopic Microsurgery (TEM) in advanced rectal cancer disease treatment [Il ruolo della TEM nel trattamento dei tumori del retto extraperitoneale]. *Ann. Ital. Di Chir.* **2010**, *81*, 269–274.

34. Quaresima, S.; Balla, A.; Dambrosio, G.; Bruzzone, P.; Ursi, P.; Lezoche, E.; Paganini, A.M. Endoluminal loco-regional resection by TEM after R1 endoscopic removal or recurrence of rectal tumors. *Minim. Invasive Ther. Allied Technol.* **2016**, *25*, 134–140. [CrossRef]

35. Lezoche, E.; Fabiani, B.; D'Ambrosio, G.; Ursi, P.; Balla, A.; Lezoche, G.; Monteleone, F.; Paganini, A.M. Nucleotide-guided mesorectal excision combined with endoluminal locoregional resection by transanal endoscopic microsurgery in the treatment of rectal tumors: Technique and preliminary results. *Surg. Endosc.* **2013**, *27*, 4136–4141. [CrossRef]

36. Legtenberg, R.; Groeneveld, A.W.; Elwenspoek, M. Comb-drive actuators for large displacements. *J. Micromech. Microeng.* **1996**, *6*, 320. [CrossRef]

37. Chen, T.; Sun, L.; Chen, L.; Rong, W.; Li, X. A hybrid-type electrostatically driven microgripper with an integrated vacuum tool. *Sens. Actuators A Phys.* **2010**, *158*, 320–327. [CrossRef]

38. Yeh, J.A.; Chen, C.N.; Lui, Y.S. Large rotation actuated by in-plane rotary comb-drives with serpentine spring suspension. *J. Micromech. Microeng.* **2004**, *15*, 201. [CrossRef]

39. Yeh, J.A.; Jiang, S.S.; Lee, C. MOEMS variable optical attenuators using rotary comb drive actuators. *IEEE Photonics Technol. Lett.* **2006**, *18*, 1170–1172. [CrossRef]

40. Kim, K.; Liu, X.; Zhang, Y.; Sun, Y. Nanonewton force-controlled manipulation of biological cells using a monolithic MEMS microgripper with two-axis force feedback. *J. Micromech. Microeng.* **2008**, *18*. [CrossRef]

41. Kim, K.; Liu, X.; Zhang, Y.; Cheng, J.; Wu, X.Y.; Sun, Y. Elastic and viscoelastic characterization of microcapsules for drug delivery using a force-feedback MEMS microgripper. *Biomed. Microdevices* **2009**, *11*, 421–427. [CrossRef]

42. Solano, B.; Wood, D. Design and testing of a polymeric microgripper for cell manipulation. *Microelectron. Eng.* **2007**, *84*, 1219–1222. [CrossRef]

43. Zeman, M.J.; Bordatchev, E.V.; Knopf, G.K. Design, kinematic modeling and performance testing of an electro-thermally driven microgripper for micromanipulation applications. *J. Micromech. Microeng.* **2006**, *16*, 1540. [CrossRef]

44. Zhang, R.; Chu, J.; Wang, H.; Chen, Z. A multipurpose electrothermal microgripper for biological micro-manipulation. *Microsyst. Technol.* **2013**, *19*, 89–97. [CrossRef]

45. Cauchi, M.; Grech, I.; Mallia, B.; Mollicone, P.; Sammut, N. The effects of cold arm width and metal deposition on the performance of a U-beam electrothermal MEMS microgripper for biomedical applications. *Micromachines* **2019**, *10*, 167. [CrossRef]

46. Cauchi, M.; Grech, I.; Mallia, B.; Mollicone, P.; Sammut, N. The effects of structure thickness, air gap thickness and silicon type on the performance of a horizontal electrothermal MEMS microgripper. *Actuators* **2018**, *7*, 38. [CrossRef]

47. Ren, H.; Wu, S.T. Adaptive Lenses Based on Soft Electroactive Materials. *Appl. Sci.* **2018**, *8*, 1085. [CrossRef]

48. Yan, B.; Wang, K.; Hu, Z.; Wu, C.; Zhang, X. Shunt damping vibration control technology: A review. *Appl. Sci.* **2017**, *7*, 494. [CrossRef]

49. Rossi, A.; Orsini, F.; Scorza, A.; Botta, F.; Belfiore, N.P.; Sciuto, S.A. A review on parametric dynamic models of magnetorheological dampers and their characterization methods. *Actuators* **2018**, *7*, 16. [CrossRef]

50. Botta, F.; Marx, N.; Gentili, S.; Schwingshackl, C.W.; Di Mare, L.; Cerri, G.; Dini, D. Optimal placement of piezoelectric plates for active vibration control of gas turbine blades: Experimental results. In Proceedings of the SPIE - The International Society for Optical Engineering, San Diego, CA, USA, 11–15 March 2012; Volume 8345.

51. Botta, F.; Dini, D.; Schwingshackl, C.; Di Mare, L.; Cerri, G. Optimal placement of piezoelectric plates to control multimode vibrations of a beam. *Adv. Acoustics Vib.* **2013**. . [CrossRef]

52. Botta, F.; Rossi, A.; Schinaia, L.; Scorza, A.; Orsini, F.; Sciuto, S.A.; Belfiore, N.P. Experimental validation on optimal placement of pzt plates for active beam multimode vibrations reduction. In Proceedings of the 23rd Conference of the Italian Association of Theoretical and Applied Mechanics AIMETA 2017, Salerno, Italy, 4–7 September 2017; Volume 3, pp. 2258–2269.

53. Botta, F.; Toccaceli, F. Piezoelectric plates distribution for active control of torsional vibrations. *Actuators* **2018**, *7*, 23. [CrossRef]

54. Xiao, Y.; Wang, B.; Zhou, S. Pull-in voltage analysis of electrostatically actuated MEMS with piezoelectric layers: A size-dependent model. *Mech. Res. Commun.* **2015**, *66*, 7–14. [CrossRef]

55. Azizi, S.; Ghodsi, A.; Jafari, H.; Ghazavi, M.R. A conceptual study on the dynamics of a piezoelectric MEMS (Micro Electro Mechanical System) energy harvester. *Energy* **2016**, *96*, 495–506. [CrossRef]

56. Madinei, H.; Khodaparast, H.H.; Adhikari, S.; Friswell, M.I.; Fazeli, M. Adaptive tuned piezoelectric MEMS vibration energy harvester using an electrostatic device. *Eur. Phys. J. Spec. Top.* **2015**, *224*, 2703–2717. [CrossRef]

57. Kanno, I. Piezoelectric MEMS for energy harvesting. *J. Phys. Conf. Ser.* **2015**, *660*. [CrossRef]

58. Tian, W.; Ling, Z.; Yu, W.; Shi, J. A review of MEMS scale piezoelectric energy harvester. *Appl. Sci.* **2018**, *8*, 645. [CrossRef]

59. Nah, S.K.; Zhong, Z.W. A microgripper using piezoelectric actuation for micro-object manipulation. *Sens. Actuators A Phys.* **2007**, *133*, 218–224. [CrossRef]

60. Haddab, Y.; Chaillet, N.; Bourjault, A. A microgripper using smart piezoelectric actuators. In Proceedings of the 2000 IEEE/RSJ International Conference on Intelligent Robots and Systems, Takamatsu, Japan, 31 October–5 November 2000; Volume 1.

61. Wang, D.H.; Yang, Q.; Dong, H.M. A monolithic compliant piezoelectric-driven microgripper: Design, modeling, and testing. *IEEE/ASME Trans. Mechatron.* **2013**, *18*, 138–147. [CrossRef]

62. Loh, O.; Vaziri, A.; Espinosa, H.D. The potential of MEMS for advancing experiments and modeling in cell mechanics. *Exp. Mech.* **2009**, *49*, 105–124. [CrossRef]

63. Crawley, E.F.; Luis, J.D. Use of piezoelectric actuators as elements of intelligent structures. *AIAA J.* **1987**, *25*, 1373–1385. [CrossRef]

64. Eom, C.B.; Trolier-McKinstry, S. Thin-film piezoelectric MEMS. *MRS Bull.* **2012**, *37*, 1007–1017. [CrossRef]

65. Xu, R.; Lei, A.; Christiansen, T.L.; Hansen, K.; Guizzetti, M.; Birkelund, K.; Thomsen, E.V.; Hansen, O. Screen printed PZT/PZT thick film bimorph MEMS cantilever device for vibration energy harvesting. In Proceedings of the 2011 16th International Solid-State Sensors, Actuators and Microsystems Conference, TRANSDUCERS'11, Beijing, China, 5–9 June 2011; pp. 679–682.

66. Shen, D.; Park, J.H.; Ajitsaria, J.; Choe, S.Y.; Wikle, H.C.; Kim, D.J. The design, fabrication and evaluation of a MEMS PZT cantilever with an integrated Si proof mass for vibration energy harvesting. *J. Micromech. Microeng.* **2008**, *18*, 055017. [CrossRef]

67. Mayrhofer, P.M.; Wistrela, E.; Kucera, M.; Bittner, A.; Schmid, U. Fabrication and characterisation of ScAlN-based piezoelectric MEMS cantilevers. In Proceedings of the 2015 Transducers—2015 18th International Conference on Solid-State Sensors, Actuators and Microsystems, TRANSDUCERS 2015, Anchorage, AK, USA, 21–25 June 2015; pp. 2144–2147.

68. Nagano, T.; Nishigaki, M.; Abe, K.; Itaya, K.; Kawakubo, T. Fabrication and performance of piezoelectric MEMS tunable capacitors constructed with AlN bimorph structure. In Proceedings of the IEEE MTT-S International Microwave Symposium Digest, San Francisco, CA, USA, 11–16 June 2006; pp. 1285–1288.

69. Park, J.S.; Yang, S.J.; Kyung-Il, L.E.E.; Kang, S.G. Fabrication and electro-mechanical characteristics of piezoelectric micro bending actuators on silicon substrates. *J. Ceram. Soc. Jpn.* **2006**, *114*, 1089–1092. [CrossRef]

70. Yuan, Y.H.; Du, H.J.; Xia, X.; Wong, Y.R. Modeling, fabrication and characterization of piezoelectric ZnO-based micro-sensors and micro-actuators. *Appl. Mech. Mater.* **2014**, *444–445*, 1636–1643. [CrossRef]

71. Lou, L.; Yu, H.; Haw, M.T.X.; Zhang, S.; Gu, Y.A. Comparative characterization of bimorph and unimorph AlN piezoelectric micro-machined ultrasonic transducers. In Proceedings of the IEEE International Conference on Micro Electro Mechanical Systems (MEMS), Shanghai, China, 24–28 January 2016; Volume 2016-February, pp. 1090–1093.

72. Zeng, Y.; Groenesteijn, J.; Alveringh, D.; Steenwelle, R.J.A.; Ma, K.; Wiegerink, R.J.; Lotters, J.C. Micro Coriolis MASS flow sensor driven by integrated PZT thin film actuators. In Proceedings of the IEEE International Conference on Micro Electro Mechanical Systems (MEMS), Belfast, UK, 21–25 January 2018; Volume 2018-January, pp. 850–853.

73. Sindhanaiselvi, D.; Shanmuganantham, T. Investigation on performance of piezoelectric beam based MEMS actuator for focussing of micro lens in mobile application. In Proceedings of the IEEE International Conference on Circuits and Systems, ICCS 2017, Thiruvananthapuram, India, 20–21 December 2017; Volume 2018-January, pp. 398–403.

74. Chen, S.H.; Michael, A.; Kwok, C.Y. A Fast Response MEMS Piezoelectric Microlens Actuator with Large Stroke and Low Driving Voltage. In Proceedings of the NEMS 2018 - 3th Annual IEEE International Conference on Nano/Micro Engineered and Molecular Systems, Singapore, Singapore, 22–26 April 2018; pp. 199–203.

75. Tsaur, J.; Zhang, L.; Maeda, R.; Matsumoto, S.; Khumpuang, S.; Wan, J. Design and fabrication of 1D and 2D micro scanners actuated by double layered PZT bimorph beams. In Proceedings of the 2001 International Microprocesses and Nanotechnology Conference, MNC 2001, Shimane, Japan, 31 October–2 November 2001; pp. 204–205.

76. Tsaur, J.; Zhang, L.; Maeda, R.; Matsumoto, S.; Khumpuang, S. Design and Fabrication of 1D and 2D Micro Scanners Actuated by Double Layered Lead Zirconate Titanate (PZT) Bimorph Beams. *Jpn. J. Appl. Phys.* **2002**, *41*, 4321–4326. [CrossRef]

77. Kuo, C.L.; Lin, S.C.; Wu, W.J. Fabrication and performance evaluation of a metal-based bimorph piezoelectric MEMS generator for vibration energy harvesting. *Smart Mater. Struct.* **2016**, *25*, 1280–1284. [CrossRef]

78. Che, L.; Halvorsen, E.; Chen, X.; Yan, X. A micromachined piezoelectric PZT-based cantilever in d33 mode. In Proceedings of the 2010 IEEE 5th International Conference on Nano/Micro Engineered and Molecular Systems, NEMS 2010, Xiamen, China, 20–23 January 2010; pp. 785–788.

79. Kanno, I. Piezoelectric MEMS: Ferroelectric thin films for MEMS applications. *Jpn. J. Appl. Phys.* **2018**, *57*. [CrossRef]

80. Strambi, G.; Barboni, R.; Gaudenzi, P. Pin-force and Euler-Bernoulli models for analysis of intelligent structures. *AIAA J.* **1995**, *33*, 1746–1749. [CrossRef]

81. Waisman, H.; Abramovich, H. Active stiffening of laminated composite beams using piezoelectric actuators. *Compos. Struct.* **2002**, *58*, 109–120. [CrossRef]

82. Botta, F.; Scorza, A.; Rossi, A. Optimal piezoelectric potential distribution for controlling multimode vibrations. *Appl. Sci.* **2018**, *8*, 551. [CrossRef]

83. Wells, P.N.; Liang, H.D. Medical ultrasound: Imaging of soft tissue strain and elasticity. *J. R. Soc. Interface* **2011**, *8*, 1521–1549. [CrossRef]